Experimental Realization of Robust Geometric Quantum Gates with Solid-State Spins

Y.-Y. Huang,[1] Y.-K. Wu,[2] F. Wang,[1] P.-Y. Hou,[1] W.-B. Wang,[1] W.-G. Zhang,[1] W.-Q. Lian,[1] Y.-Q. Liu,[1] H.-Y. Wang,[1] H.-Y. Zhang,[1] L. He,[1] X.-Y. Chang,[1] Y. Xu,[1] and L.-M. Duan[1,2,*]

[1]*Center for Quantum Information, IIIS, Tsinghua University, Beijing 100084, People's Republic of China*

[2]*Department of Physics, University of Michigan, Ann Arbor, Michigan 48109, USA*

(Received 1 May 2018; published 9 January 2019)

We experimentally realize a universal set of single-bit and two-bit geometric quantum gates by adiabatically controlling solid-state spins in a diamond defect. Compared with the nonadiabatic approach, the adiabatic scheme for geometric quantum computation offers a unique advantage of inherent robustness to parameter variations, which is explicitly demonstrated in our experiment by showing that the single-bit gates remain unchanged when the driving field amplitude varies by a factor of 2 or the detuning fluctuates in a range comparable to the inverse of the gate time. The reported adiabatic control technique and its convenient implementation offer a paradigm for achieving quantum computation through robust geometric quantum gates, which is important for quantum information systems with parameter-fluctuation noise such as those from the inhomogeneous coupling or the spectral diffusion.

DOI: 10.1103/PhysRevLett.122.010503

Introduction.—When a quantum system undergoes a cyclic evolution in a parameter space, a nondegenerate quantum state picks up not only a dynamical phase but also a geometric phase [1]. Different from the dynamical phase that depends on the energy of a state, a geometric phase is solely related to the geometric structure of the enclosed path. For degenerate states, the geometric phase is replaced with a geometric unitary operator [2], termed as the holonomy in differential geometry. The geometric phase or the holonomy plays a key role in many physical phenomena and applications, such as topological effects [3] and the engineering of artificial gauge fields in cold atoms [4].

An important application of holonomies is to realize all-geometric quantum computation [5,6], whose basic requirement is a universal set of geometric quantum gates, containing a non-Abelian set of single-bit and two-bit operations. By use of nonadiabatic cyclic evolutions [7], recent experiments have reported the realization of non-Abelian single-qubit operations [8–10] and a universal set of quantum gates [11,12] by nonadiabatic geometric means in several physical systems. A related but different-concept geometric gate has also been realized earlier with two coupled ions using nonadiabatic laser manipulation of the ions' motion [13]. In the adiabatic approach to geometric quantum computation, the gates only depend on the ratio of parameters and are therefore robust to fluctuation of their absolute values [5,6,14–18]. This important advantage, however, is not shared by the nonadiabatic approach [7–12]. To implement the adiabatic geometric gates, schemes have been proposed in several physical systems, including trapped ions [16], superconducting qubits [17], and quantum dots [18]. In experiments, single-qubit adiabatic geometric rotation along the z axis has been realized with an electron spin resonance system [14]. Non-Abelian single-bit adiabatic geometric gates have been realized recently with a trapped ion [15], and this realization requires manipulation of four coupled levels following the approach in [16] and cannot be easily extended to other systems due to its level complication. The realization of a universal set of both single-bit and two-bit entangling gates all by adiabatic geometric means in a single experiment is still lacking due to the challenging requirement of exquisite control of complicated level structure.

Here, we report the realization of both single-bit and two-bit geometric quantum gates, which together make a universal gate set, all by adiabatically manipulating solid-state spins of a diamond defect using a significantly simplified level structure. We achieve high gate fidelities and demonstrate explicitly in experiments that all the single-bit geometric gates are robust against significant parameter variations in the coupling rate and the frequency detuning, which are an important source of noise for some quantum information platforms.

Implementation of geometric quantum gates through adiabatic evolution.—We consider a paradigmatic Hamiltonian describing a spin in an external magnetic field

$$H_B(t) = \boldsymbol{B}(t)\cdot\boldsymbol{\sigma}, \tag{1}$$

where $\boldsymbol{\sigma}$ is a vector of Pauli matrices and $\boldsymbol{B}(t) = B(t)\boldsymbol{n}(t)$ with $\boldsymbol{n}(t) = \sin\theta(t)\cos\phi(t)\boldsymbol{e}_x + \sin\theta(t)\sin\phi(t)\boldsymbol{e}_y + \cos\theta(t)\boldsymbol{e}_z$ varying adiabatically in time. The Hamiltonian has two instantaneous eigenstates $|\Psi_-(t)\rangle = \sin[\theta(t)/2]e^{-i\phi(t)}|0\rangle - \cos[\theta(t)/2]|1\rangle$ and $|\Psi_+(t)\rangle = \cos[\theta(t)/2]|0\rangle + \sin[\theta(t)/2]e^{i\phi(t)}|1\rangle$ with eigenenergies being $E_\pm(t) = \pm B(t)$. As we

vary the parameter $\boldsymbol{B}$ adiabatically and cyclically, a state initially prepared at the eigenstate $|\Psi_\pm(0)\rangle$ ends up acquiring both a dynamical phase and a geometric phase, i.e.,

$$|\Psi_\pm(\tau)\rangle = e^{\mp i(\gamma_g+\gamma_d)}|\Psi_\pm(0)\rangle, \tag{2}$$

where $\gamma_d = \int_0^\tau E_+(t)dt$ is the dynamical phase and $\gamma_g = -i\int_0^\tau dt\langle\Psi_+(t)|\partial_t|\Psi_+(t)\rangle$ is the geometric phase. By varying the direction $\boldsymbol{n}_0 \equiv \boldsymbol{n}(t=0)$, we can set $|\Psi_\pm(0)\rangle$ as eigenstates of noncommuting operators in different cycles, and hence realize non-Abelian holonomies when composing these cycles. In our experiment, we are able to remove the dynamical phase γ_d by suddenly tuning a control microwave pulse [19], ending up with a purely geometric unitary operation

$$U = e^{-i\gamma_g \boldsymbol{n}_0\cdot\boldsymbol{\sigma}}, \tag{3}$$

a rotation around the $\boldsymbol{n}_0$ axis. By selecting $\boldsymbol{n}_0$ appropriately, we can realize a universal set of single-qubit quantum operations, $Z_{\pi/2}$, $Z_{\pi/8}$, and $X_{\pi/2}$, corresponding to rotations with respect to the z and x axes, respectively.

In our experiment, we realize a universal set of all-geometric quantum gates including single-qubit and controlled π-rotation (CROT) operations by controlling solid-state spins in a diamond defect at room temperature. The electron and nuclear spins around the negatively charged nitrogen vacancy (NV) center in the diamond are used to realize a local quantum spin register [20], which, combined with the photonic coupling between remote quantum registers [21,22], provides a scalable system for solid-state quantum information processing [23,24]. The NV center possesses a spin triplet ground state with a zero-field splitting $D = 2.87$ GHz between $m_s = 0$ and $m_s = \pm 1$ states. Under an magnetic field $B_z = 502$ G, which is tuned to be along the NV axis through the angle-sensitive fluorescence counts [25], the degeneracy of two states with $m_s = \pm 1$ is lifted. We can therefore select $|m_s = 0\rangle \equiv |0\rangle$ and $|m_s = -1\rangle \equiv |1\rangle$ states as the computational basis. The spin state is initialized to the $|0\rangle$ level by optical pumping and read out by identifying distinct fluorescence levels of the states after a short illumination of a green laser pulse [20].

We apply microwave pulses to couple the $|0\rangle$ and $|1\rangle$ qubit states as shown in Fig. 1; the coupling can be described by the Hamiltonian

$$H(t) = \frac{\Omega(t)}{2}\sigma_x - \frac{\Delta(t)}{2}\sigma_z, \tag{4}$$

where $\Omega(t)$ is the Rabi frequency and $\Delta(t)$ is the detuning defined as $\Delta(t) = \omega(t) - \omega_0$ with $\omega(t)$ being the frequency of the microwave pulse and $\omega_0 = D - \gamma_e B_z$ ($\gamma_e = 2.8$ MHz/G) being the energy difference between the $|0\rangle$ and $|1\rangle$ levels. Here $\hbar$ is set to 1. Both $\Omega(t)$ and $\Delta(t)$ can be readily tuned through an arbitrary waveform generator.

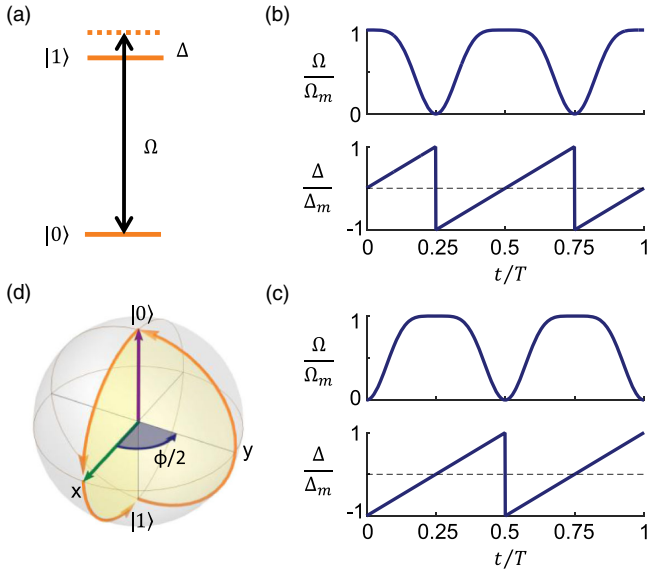

FIG. 1. Relevant energy levels and microwave shape schemes for the adiabatic geometric single-qubit gates in a diamond NV center. (a) The relevant energy level structure of the electron spin in an NV center under a magnetic field. The two levels encoding a qubit are coupled by a microwave pulse with the Rabi frequency Ω and the detuning Δ. (b) The microwave pulse shape used to achieve a geometric single-qubit rotation operation along the x axis. $\Omega(t)$ is in the form of $\Omega(t)/\Omega_m = 1 - |\sin(2\pi t/T)|^n$ [26] with Ω_m, T, and n being the maximum value of $|\Omega|$, the gate time, and a positive integer, respectively. We take $n = 5$ for our experiment. $\Delta(t)$ consists of piecewise linear functions of time with the sign being suddenly reversed at $t = T/4$ and $3T/4$ and Δ_m is its maximal value. Phase shifts $\Delta\phi_1 = \pi + \phi/2$ and $\Delta\phi_2 = -\pi - \phi/2$ are inserted into the microwave at $t = T/4$ and $3T/4$, respectively. (c) The microwave pulse shape used to realize a rotation operation about the z axis. A phase $\Delta\phi = \pi + \phi/2$ is inserted into the microwave at $t = T/2$. (d) Evolution of a state initialized to an instantaneous eigenstate of the Hamiltonian (4) in the Bloch sphere, showing the geometric phase which equals half of the enclosed solid angle ϕ. The green and purple arrows denote the initial eigenstate respectively for scheme shown in (b),(c).

In our experiment, we realize geometric rotation gates $X_{\pi/2}$, $Z_{\pi/2}$, and $Z_{\pi/8}$ through adiabatic manipulation of $\Delta(t)$ and $\Omega(t)$. The former two gates, when combined, give the Hadamard gate H and the NOT gate N as $H = X_{\pi/2}Z_{\pi/2}X_{\pi/2}$ and $N = X_{\pi/2}^2$, which, together with the $\pi/8$ gate $A = Z_{\pi/8}$, make a universal set of single-qubit gates. In order to perform the $X_{\pi/2}$ gate, we adiabatically tune $|\Omega(t)|$ and $\Delta(t)$ following the scheme shown in Fig. 1(b); this type of pulse is known as the BIR-4 pulse in nuclear magnetic resonance [27]. At $t = T/4$ and $3T/4$, phase shifts $\Delta\phi_1 = \pi + \phi/2$ and $\Delta\phi_2 = -\pi - \phi/2$ are suddenly imprinted in the microwave pulse, respectively, with the sign of Δ being flipped simultaneously. While this sudden tuning flips the sign of the coupling Hamiltonian, the state remains

unchanged. If a state is initialized to an instantaneous eigenstate, it remains an eigenstate of the new flipped Hamiltonian but with the opposite energy. So the adiabaticity of the state evolution is maintained. The abrupt change of the sign of energy enables us to remove the contribution from the dynamical phase in an entire cycle. The state finally picks up only a geometric phase $\gamma_g = \phi/2$ as illustrated in Fig. 1(d). We see from Eq. (3) that a rotation operator X_ϕ is realized under the cyclic evolution. When we set $\phi = \pi/2$, we make an $X_{\pi/2}$ operator. For the adiabatic condition [28] to be satisfied, we vary $H(t)$ slowly to make sure $Q \equiv \{[2(\Delta^2(t) + \Omega^2(t))^{3/2}]/[|\dot{\Omega}(t)\Delta(t) - \Omega(t)\dot{\Delta}(t)|]\} \gg 1$. In our experiments we have $Q > 12$ for all the geometric gates.

Analogous to the $X_{\pi/2}$ gate, we realize the geometric $Z_{\pi/2}$ and $Z_{\pi/8}$ gates using the pulse shape shown in Fig. 1(c). At $t = T/2$, a phase of $\pi + \phi/2$ is suddenly introduced into the microwave pulse and the sign of Δ is flipped, resulting in a rotation operation about the z axis: Z_ϕ. The $Z_{\pi/2}$ and $Z_{\pi/8}$ gates are implemented when we take $\phi = \pi/2$ and $\pi/8$, respectively.

Experiments results for non-Abelian single-qubit geometric gates.—To characterize these geometric gates, we apply them to distinct initial electron spin states and measure the final states with quantum state tomography [29]. We find the state fidelity $(98.2 \pm 0.4)\%$, $(98.9 \pm 0.3)\%$, and $(97.5 \pm 0.5)\%$, respectively, for the $Z_{\pi/2}$, $Z_{\pi/8}$, and $X_{\pi/2}$ gates, which are obtained by averaging the results for six complementary initial states as shown in Fig. 2(b). The major contribution to the infidelity comes from the state preparation and detection errors, which can be separately detected by the randomized benchmarking method [30]. For the randomized benchmarking, we concatenate m random dynamical Clifford gates generated by $\{I, X_{\pm\pi/2}, X_\pi, Y_{\pm\pi/2}, Y_\pi\}$, and a specific recovery Clifford gate, and average the fidelities over 20 different series of operations. Figure 2(a) shows the fidelity decay as the number of gates increases. The decay is fitted using the function $F = Ap^m + B$, where A and B absorb the preparation and measurement error and p represents the reference decay rate. We find $p = 0.986 \pm 0.002$ from fitting. The intrinsic gate error can be calculated by $r = (1-p)(d-1)/d$ with $d = 2^n$ and n being the number of qubits. The reference Clifford gate fidelity is $F = 1 - r/1.875 = 0.996(1)$. To measure the target gate fidelity, we interleave m target gates following each series of random gates mentioned above for randomized benchmarking and examine the fidelity decay when increasing the number of gates. By fitting the data, we find the decay rate of the target gate to be $p_{Z_{\pi/2}} = 0.969 \pm 0.004$ and $p_{X_{\pi/2}} = 0.950 \pm 0.008$, respectively, and get the gate error by $r_{\text{gate}} = (1 - p_{\text{gate}}/p)(d-1)/d$, giving the target gate fidelity $F_{Z_{\pi/2}} = 0.991 \pm 0.002$, $F_{X_{\pi/2}} = 0.982 \pm 0.004$ [Fig. 2(a)]. The fidelities are mainly limited here by the dephasing time $T_2^* = 2.5\ \mu$s for our diamond sample with $1.1\%C^{13}$ concentration. We expect that the gate fidelity will be significantly improved with an isotopically purified diamond sample which has T_2^* in the range of tens of microseconds [31,32].

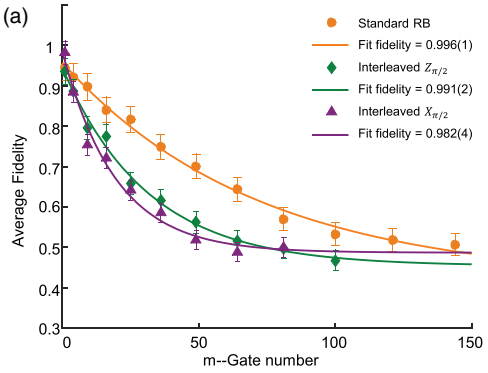

(b)

Fidelities of single-qubit adiabatic gates measured by quantum state tomography							
Initial state	$\|0\rangle$	$\|1\rangle$	$\|0\rangle+\|1\rangle$	$\|0\rangle-i\|1\rangle$	$\|0\rangle-\|1\rangle$	$\|0\rangle+i\|1\rangle$	Average
$Z_{\pi/2}$ gate fidelity	0.988(8)	0.97(1)	0.975(7)	0.992(5)	0.98(1)	0.993(4)	0.98(1)
$Z_{\pi/8}$ gate fidelity	0.996(5)	0.97(1)	0.998(7)	0.992(2)	0.997(4)	0.98(1)	0.988(7)
$X_{\pi/2}$ gate fidelity	0.96(2)	0.98(1)	0.983(6)	0.98(1)	0.959(7)	0.98(1)	0.97(1)

FIG. 2. Measured fidelity for the adiabatic geometric singe-qubit gates. (a) Average fidelity as a function of the number of gates. Orange circles, green diamonds, and purple triangles denote the results from a standard randomized benchmarking (RB) protocol, a interleaved $Z_{\pi/2}$ and a interleaved $X_{\pi/2}$ gate, respectively. Each point in the figure is obtained by averaging the experimental data from 20 measurements. These points are fitted by $F = Ap^m + B$ plotted as solid lines with the corresponding colors. (b) Fidelity of the final states measured by the quantum state tomography for $Z_{\pi/2}$, $Z_{\pi/8}$, and $X_{\pi/2}$ gates acting on six distinct initial states. For each gate, the parameters of microwave pulses are $T = 1\ \mu s$, $\Omega_m = 20$ MHz, and $\Delta_m = 20$ MHz. Note that the number in the bracket following the fidelity value represents the error bar (s.d.) in the last decimal place.

Robustness of adiabatic geometric single-qubit gates.—The adiabatic geometric scheme ensures the robustness of the realized gates against the variation noise of the microwave amplitude Ω_m and the spectral diffusion δ, which can be caused, for instance, by the randomness in the coupling rate or the spectral diffusion, an important source of noise for some solid-state systems. This robustness can be seen from Eq. (3) that a single-qubit operation is solely determined by the initial direction $\boldsymbol{n}_0$ and the Berry phase $\gamma_g = \phi/2$. For Z_ϕ, it is irrelevant to variations of Ω_m and δ. For X_ϕ, while the initial direction $\boldsymbol{n}_0$ can be slightly changed by fluctuations of δ, this effect can be strongly suppressed by taking a large Ω_m. In experiments, to evaluate this robustness for both X and Z gates, we measure the final state as a function of the imprinted phase ϕ as we vary the values of Ω_m and δ, where the detuning is modeled by $\Delta(t) + \delta$. We plot the results in Fig. 3, demonstrating that the final state characterized by the normalized photon luminance remains almost the same as Ω_m varies up to

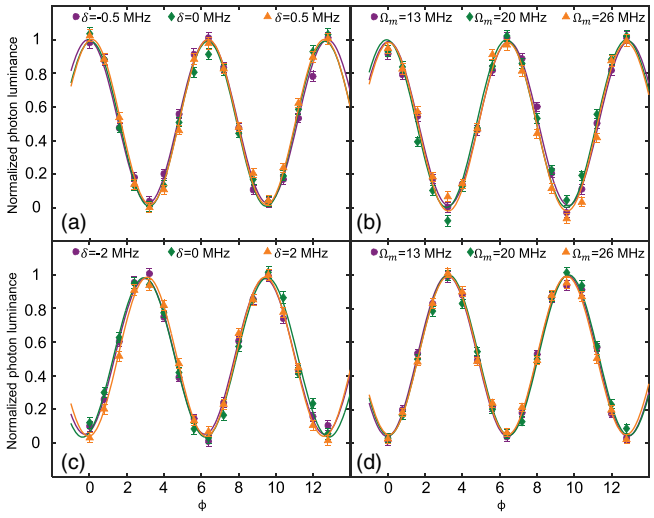

FIG. 3. Experimental results demonstrating robustness of adiabatic geometric single-qubit gates with respect to variations of Ω_m (the random coupling) and δ (the spectral diffusion). The detuning is modeled by $\Delta(t)+\delta$. Normalized photon luminance as a function of the imprinted phase ϕ under three distinct values of δ and Ω_m, respectively, for the rotation operation along the x axis (a),(b) and the rotation operation along the z axis (c),(d). The other parameters are $\Delta_m = 20$ MHz, $T = 1$ μs, and $\Omega_m = 20$ MHz in (a),(c), while in (b),(d) $\Delta_m = 20$ MHz, $T = 1$ μs, and $\delta = 0$ MHz. Note that for the Z rotation gate, two half π pulses around the x axis are applied in front and after the target gate in order to transfer the phase information to the photon luminance count.

twice or δ fluctuates with $\delta \gtrsim 1/T$. This confirms the resilience of our implemented gates. We would like to emphasize that our adiabatic results are in stark contrast to nonadiabatic ones in previous experiments, where the amplitude of microwave or optical pulses and their detuning are required to be precisely calibrated and controlled for achieving high-fidelity gates [8–12,33].

Experiments results for entangling geometric gates.—To implement the geometric quantum two-qubit CROT gate, we use a nearby C^{13} nuclear spin as a control qubit with two basis vectors denoted by $|\uparrow\rangle$ and $|\downarrow\rangle$ and the NV center electron spin as a target qubit. The system is initially polarized to the $|0,\uparrow\rangle$ state through optical pumping under a 502 G magnetic field along the NV axis [34,35]. To drive the state $|0,\downarrow\rangle$ out of our computational space, leaving behind the $|0,\uparrow\rangle$ state, we further apply a MW0 pulse to excite the $|0,\downarrow\rangle$ state to the irrelevant $|a,\downarrow\rangle$ level ($|a\rangle \equiv |m_s = +1\rangle$ is used as an ancillary level) as shown in Fig. 4(a). Under the control microwave pulse, the effective Hamiltonian of the two-bit system has the form [11,33]

$$H_2 = H_\uparrow + H_\downarrow, \tag{5}$$

where

$$H_\sigma = \frac{\Omega(t)}{2}(|1\sigma\rangle\langle 0\sigma| + \text{H.c.}) - \frac{\Delta_\sigma(t)}{2}(|0\sigma\rangle\langle 0\sigma| - |1\sigma\rangle\langle 1\sigma|), \tag{6}$$

with $\sigma = \uparrow, \downarrow$, $\Delta_\downarrow = \Delta_\uparrow - \omega_1$, and $\omega_1 = 13.7$ MHz in our experiment, which is the difference between the frequency of the resonant MW2 and MW1 as displayed in Fig. 4(a). We can apply the same microwave pulse as shown in Fig. 1(b) to achieve an X_π gate between the $|0\uparrow\rangle$ and $|1\uparrow\rangle$ levels without creating a geometric phase for a state in the subspace of $|0\downarrow\rangle$ and $|1\downarrow\rangle$ if $\Delta_\uparrow < \omega_1$ is always satisfied. However, this method generates a dynamical phase for a state in the latter subspace. To remove this phase, we insert two spin echoes at $t = T/4$ and $3T/4$, as shown in Fig. 4(b) (see Methods for the realization of a controlled rotation gate). This exactly achieves a CROT gate:

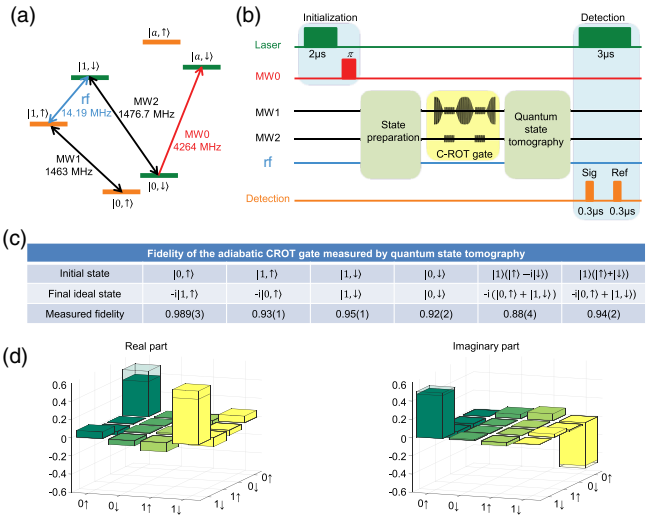

FIG. 4. Level scheme, pulse sequence, and experimental results for the geometric two-qubit CROT gate. (a) Energy level structure of the electron and nuclear spins for the geometric CROT gate together with microwave and radio-frequency (rf) coupling configuration. (b) Time sequence for implementing and detecting the CROT gate. We first use a MW0 π pulse followed by illumination of a 532 nm green laser pulse for 2 μs to initialize the system and then apply MW1, MW2, and rf pulses to create a desired state. The spin echo for implementation of the geometric CROT gate is realized by simultaneously applying two π pulses denoted as MW1 and MW2. Other parameters for the CROT gate are $n = 5$, $T = 2$ μs, $\Delta_m = 7$ MHz, and $\Omega_m = 4$ MHz. Two-qubit quantum state tomography is used to measure the fidelity of the final state. To avoid the decoherence of the electron spin during the slow RF pulse, a spin echo of 1 MHz is inserted in the middle of the quantum state tomography process. (c) Measured fidelity of the final states after applying the CROT gate to six complementary initial states. (d) Measured real and imaginary parts of the final state matrix elements for the geometric CROT gate applied to the initial state $|1\rangle(|\uparrow\rangle + |\downarrow\rangle)$ compared with the matrix elements under the ideal gate represented by the hollow caps.

a rotation about the x axis for an electron spin only when a nuclear spin is in the $|\uparrow\rangle$ level.

To characterize the CROT gate, we initialize the two-qubit system to six complementary states and measure the fidelity of the final states with quantum state tomography after applying a CROT gate to these states. The results are listed in Fig. 4(c). For a typical initial product state $|1\rangle(|\uparrow\rangle + |\downarrow\rangle)$, the CROT gate generates entanglement, yielding an entangled final state $-i|0\uparrow\rangle + |1\downarrow\rangle$ with a measured fidelity of $(94 \pm 2)\%$, slightly higher than the fidelity of CNOT gate realized with nonadiabatic geometric pulses [11]. In Fig. 4(d), we also show the measured state matrix elements after the geometric CROT gate, demonstrating good agreement with those under the ideal gate. Our scheme for the adiabatic geometric gate by itself is also robust to the parameter variation errors similar to the single-bit case. However, in our experiment we also need to apply spin echo pulses to prolong the system coherence time for the two-bit gate, and these echo pulses are not intrinsically robust if we do not have a very high amplitude for the microwave field which is the case here. In the Supplemental Material [36], we show by numerical simulation that if we neglect the errors of the ancillary echo pulses, the adiabatic geometric gate by itself is very robust to the parameter variation errors.

Summary.—We have realized a non-Abelian set of single-qubit and two-qubit adiabatic geometric quantum gates with solid-state spins and demonstrate the unique robustness of adiabatic gates to parameter variations. Our technique to implement robust geometric quantum gates based on convenient level configurations may also find application in other scalable quantum systems, such as trapped ions or superconducting qubits.

This work was supported by Ministry of Education of China and the National key Research and Development Program of China (2016YFA0301902). L. M. D. and Y. K. W. acknowledge in addition support from the AFOSR MURI and the ARL CDQI program and Y. X. acknowledges support from the Tsinghua start up program and the National Thousand-Young-Talents Program.

*lmduan@tsinghua.edu.cn

[1] M. V. Berry, Proc. R. Soc. A **392**, 45 (1984).
[2] F. Wilczek and A. Zee, Phys. Rev. Lett. **52**, 2111 (1984).
[3] D. Xiao, M. C. Chang, and Q. Niu, Rev. Mod. Phys. **82**, 1959 (2010).
[4] J. Dalibard, F. Gerbier, G. Juzeliunas, and P. Ohberg, Rev. Mod. Phys. **83**, 1523 (2011).
[5] P. Zanardi and M. Rasetti, Phys. Lett. A **264**, 94 (1999).
[6] J. Pachos, P. Zanardi, and M. Rasetti, Phys. Rev. A **61**, 010305(R) (1999).
[7] E. Sjoqvist, D. M. Tong, L. Mauritz Andersson, B. Hessmo, M. Johansson, and K. Singh, New J. Phys. **14**, 103035 (2012).
[8] A. A. Abdumalikov, J. M. Fink, K. Juliusson, M. Pechal, S. Berger, A. Wallraff, and S. Filipp, Nature (London) **496**, 482 (2013).
[9] S. Arroyo-Camejo, A. Lazariev, S. W. Hell, and G. Balasubramanian, Nat. Commun. **5**, 4870 (2014).
[10] B. B. Zhou, P. C. Jerger, V. O. Shkolnikov, F. J. Heremans, G. Burkard, and D. D. Awschalom, Phys. Rev. Lett. **119**, 140503 (2017).
[11] C. Zu, W.-B. Wang, L. He, W.-G. Zhang, C.-Y. Dai, F. Wang, and L.-M. Duan, Nature (London) **514**, 72 (2014).
[12] G. Feng, G. Xu, and G. Long, Phys. Rev. Lett. **110**, 190501 (2013).
[13] D. Leibfried, B. DeMarco, V. Meyer, D. Lucas, M. Barrett, J. Britton, W. M. Itano, B. Jelenkovi, C. Langer, T. Rosenband, and D. J. Wineland, Nature (London) **422**, 412 (2003).
[14] H. Wu, E. M. Gauger, R. E. George, M. Mottonen, H. Riemann, N. V. Abrosimov, P. Becker, H. Pohl, K. M. Itoh, M. L. W. Thewalt, and J. J. L. Morton, Phys. Rev. A **87**, 032326 (2013).
[15] K. Toyoda, K. Uchida, A. Noguchi, S. Haze, and S. Urabe, Phys. Rev. A **87**, 052307 (2013).
[16] L. M. Duan, J. I. Cirac, and P. Zoller, Science **292**, 1695 (2001).
[17] G. Falci, R. Fazio, G. Massimo Palma, J. Siewert, and V. Vedral, Nature (London) **407**, 355 (2000).
[18] P. Solinas, P. Zanardi, N. Zanghi, and F. Rossi, Phys. Rev. A **67**, 062315 (2003).
[19] Z. H. Peng, H. F. Chu, Z. D. Wang, and D. N. Zheng, J. Phys. Condens. Matter **21**, 045701 (2009).
[20] M. W. Doherty, N. B. Manson, P. Delaney, F. Jelezko, J. Wrachtrup, and L. C. L. Hollenberg, Phys. Rep. **528**, 1 (2013).
[21] W. Pfaff, B. J. Hensen, H. Bernien, S. B. van Dam, M. S. Blok, T. H. Taminiau, M. J. Tiggelman, R. N. Schouten, M. Markham, D. J. Twitchen, and R. Hanson, Science **345**, 532 (2014).
[22] A. Sipahigil, R. E. Evans, D. D. Sukachev, M. J. Burek, J. Borregaard, M. K. Bhaskar, C. T. Nguyen, J. L. Pacheco, H. A. Atikian, C. Meuwly, R. M. Camacho, F. Jelezko, E. Bielejec, H. Park, M. Lonar, and M. D. Lukin, Science **354**, 847 (2016).
[23] L. Jiang, J. M. Taylor, A. S. Sorensen, and M. D. Lukin, Phys. Rev. A **76**, 062323 (2007).
[24] L. M. Duan and C. Monroe, Rev. Mod. Phys. **82**, 1209 (2010).
[25] R. J. Epstein, F. M. Mendoza, Y. K. Kato, and D. D. Awschalom, Nat. Phys. **1**, 94 (2005).
[26] E. Kupce and R. Freeman, J. Magn. Reson., Ser. A **115**, 273 (1995).
[27] A. Tannus and M. Garwood, NMR Biomed. **10**, 423 (1997).
[28] B. R. Holstein, Am. J. Phys. **57**, 1079 (1989).
[29] A. G. White, A. Gilchrist, G. J. Pryde, J. L. OBrien, M. J. Bremner, and N. K. Langford, J. Opt. Soc. Am. B **24**, 172 (2007).
[30] R. Barends, J. Kelly, A. Megrant, A. Veitia, D. Sank, E. Jeffrey, T. C. White, J. Mutus, A. G. Fowler, B. Campbell, Y. Chen, Z. Chen, B. Chiaro, A. Dunsworth, C. Neill, P. Omalley, P. Roushan, A. Vainsencher, J. Wenner, A. N. Korotkov *et al.*, Nature (London) **508**, 500 (2014).

[31] G. Balasubramanian1, P. Neumann, D. Twitchen, M. Markham, R. Kolesov, N. Mizuochi, J. Isoya, J. Achard, J. Beck, J. Tissler, V. Jacques, P. R. Hemmer, F. Jelezko, and J. Wrachtrup, Nat. Mater. **8**, 383 (2009).

[32] T. Ishikawa, K. C. Fu, C. Santori, V. M. Acosta, R. G. Beausoleil, H. Watanabe, S. Shikata, and K. M. Itoh, Nano Lett. **12**, 2083 (2012).

[33] X. Rong, J. Geng, F. Shi, Y. Liu, K. Xu, W. Ma, F. Kong, Z. Jiang, Y. Wu, and J. Du, Nat. Commun. **6**, 8748 (2015).

[34] V. Jacques, P. Neumann, J. Beck, M. Markham, D. Twitchen, J. Meijer, F. Kaiser, G. Balasubramanian, F. Jelezko, and J. Wrachtrup, Phys. Rev. Lett. **102**, 057403 (2009).

[35] B. Smeltzer, L. Childress, and A. Gali, New J. Phys. **13**, 025021 (2011).

[36] See Supplemental Material at http://link.aps.org/supplemental/10.1103/PhysRevLett.122.010503 for experimental setup and details for realization of geometric gates.